

1  
2  
3 **In Situ Focused Ion Beam Scanning Electron Microscope Study of Microstructural Evolution**  
4  
5 **of Single Tin Particle Anode for Li-Ion Batteries**  
6  
7  
8  
9

10  
11 Xinwei Zhou<sup>1,2</sup>, Tianyi Li<sup>1</sup>, Yi Cui<sup>1</sup>, Yongzhu Fu<sup>3</sup>, Yuzi Liu<sup>2\*</sup>, and Likun Zhu<sup>1\*</sup>  
12  
13

14  
15 <sup>1</sup>Department of Mechanical and Energy Engineering, Indiana University Purdue University  
16

17  
18 Indianapolis, Indianapolis, IN 46202  
19

20  
21 <sup>2</sup>Center for Nanoscale Materials, Argonne National Laboratory, 9700 South Cass Avenue, Argonne,  
22

23  
24 Illinois 60439  
25

26  
27 <sup>3</sup>College of Chemistry and Molecular Engineering, Zhengzhou University, Zhengzhou, Henan  
28

29  
30 450001, China  
31  
32  
33  
34  
35  
36  
37  
38  
39  
40  
41  
42  
43  
44  
45  
46  
47  
48

49 \*Corresponding author: [likzhu@iupui.edu](mailto:likzhu@iupui.edu) (L. Zhu), [yuziliu@anl.gov](mailto:yuziliu@anl.gov) (Y. Liu)  
50  
51  
52  
53  
54  
55

---

This is the author's manuscript of the article published in final edited form as:

Zhou, X., Li, T., Cui, Y., Fu, Y., Liu, Y., & Zhu, L. (2019). In Situ Focused Ion Beam Scanning Electron Microscope Study of Microstructural Evolution of Single Tin Particle Anode for Li-Ion Batteries. ACS Applied Materials & Interfaces. <https://doi.org/10.1021/acsami.8b13981>

**Abstract**

Tin (Sn) is a potential anode material for high energy density Li-ion batteries due to its high capacity, safety, abundance and low cost. However, Sn suffers from large volume change during cycling, leading to fast degradation of the electrode. For the first time, the microstructural evolution of micrometer-sized single Sn particle was monitored by focused-ion beam (FIB) polishing and scanning electron microscopy (SEM) imaging during electrochemical cycling by in situ FIB-SEM. Our results show the formation and evolution of cracks during lithiation, evolution of porous structure during delithiation and volume expansion/contraction during cycling. The electrochemical performance and the microstructural evolution of the Sn micro-particle during cycling are directly correlated, which provides insights for understanding Sn-based electrode materials.

Keywords: Li-ion battery, single tin particle battery, in situ, focused-ion beam-scanning electron microscopy, microstructural evolution

1  
2  
3 Tin (Sn) has been considered a promising anode material for lithium-ion (Li-ion) batteries  
4  
5 because it is non-toxic, abundant, and inexpensive and it has a theoretical specific capacity of 994  
6  
7 mAh g<sup>-1</sup>.<sup>1</sup> However, Sn electrode has large volume change during lithiation and delithiation, which  
8  
9 causes pulverization of active material, leading to fast capacity fading.<sup>2-4</sup> In order to address this issue,  
10  
11 it is necessary to understand the microstructure evolution and electrochemical performance of Sn  
12  
13 electrodes during cycling. In recent years, several advanced techniques have been developed to  
14  
15 investigate the microstructural evolution of anode materials during cycling in in situ and in operando  
16  
17 cell setups, such as transmission X-ray microscopy (TXM)<sup>5-9</sup> and transmission electron microscopy  
18  
19 (TEM).<sup>10-13</sup> By using synchrotron TXM, either 2D projection images or 3D microstructures have been  
20  
21 obtained to reveal the microstructure change of Sn particles during cycling.<sup>5, 8-9, 14</sup> However, the Sn  
22  
23 electrodes used in these in situ studies were composed of Sn particles with different size and shapes.  
24  
25 It is challenging to correlate the microstructural evolution of single Sn particle with the  
26  
27 electrochemical performance of the whole cell on the multiple-particle scale. Since its first application  
28  
29 for battery research in 2010,<sup>15</sup> in situ TEM has made significant contribution to reveal the  
30  
31 microstructural evolution and phase change of electrode materials.<sup>10-13</sup> Although in situ TEM allows  
32  
33 real time microstructure investigation at atomic scale resolution, the in situ cell rarely shows  
34  
35 electrochemical performance of electrodes mainly due to the size of the samples and the  
36  
37 corresponding ultralow capacity. To correlate the microstructural evolution and the electrochemical  
38  
39 performance, micrometer-sized particles have to be used, which is too big for the TEM analysis and  
40  
41 too small for X-ray characterizations in many cases. But it is appropriate for scanning electron  
42  
43 microscopy (SEM) imaging. Recently, in situ and in operando SEM have been used to obtain the  
44  
45 dynamic morphology change of battery materials.<sup>16-18</sup> Miller et. al developed an approach to carry  
46  
47 out in situ SEM of single Li-ion battery cathode particles during electrochemical cycling using a  
48  
49  
50  
51  
52  
53  
54  
55  
56  
57  
58  
59  
60

1  
2 focused-ion beam-scanning electron microscope (FIB-SEM).<sup>18</sup> In this study, we adopted and  
3  
4 optimized the approach to build a single Sn particle battery in the chamber of FIB-SEM. The  
5  
6 microstructural evolution of a single Sn micrometer-sized particle was monitored by SEM and  
7  
8 coupled with electrochemical characterizations.  
9  
10  
11  
12  
13  
14  
15  
16

17 The experiment was performed on a Zeiss Nvision 40 FIB-SEM at the Center for Nanoscale  
18  
19 Materials, Argonne National Laboratory. The schematic of experiment setup is shown in Figure 1a.  
20  
21 Figures 1b and c show the SEM images of the single Sn particle battery inside the FIB-SEM chamber.  
22  
23 To build the single particle battery cell, a Sn particle (Sigma-Aldrich) was attached to the tungsten  
24  
25 probe by ion beam carbon deposition as positive electrode. The Li metal was placed on top of the  
26  
27 SEM stub as negative electrode. One drop of ionic liquid electrolyte (ILE) was placed on top of Li  
28  
29 metal. The ILE was made by dissolving the Li salt, lithium bis (trifluoromethylsulfonyl) imide  
30  
31 (LiTFSI) (Sigma-Aldrich), in a solvent of 1-butyl-1-methylpyrrolidinium bis  
32  
33 (trifluoromethylsulfonyl) imide (P<sub>14</sub>TFSI) (Sigma-Aldrich).<sup>12, 19</sup> The vapor pressure of P<sub>14</sub>TFSI is  
34  
35 close to zero, which makes the liquid suitable for the vacuum environment in FIB-SEM.<sup>20</sup> The single  
36  
37 particle battery cycling was controlled by a Keithley 6430 sub-femtoamp remote sourcemeter from  
38  
39 Tektronix. The particle was immersed in the ILE drop during cycling and lifted out for imaging at  
40  
41 different states of charge and discharge. In order to visualize the microstructure change of the particle,  
42  
43 the imaging area was polished by FIB to remove ILE on the surface. The electron beam and ion beam  
44  
45 remain closed other than taking images. Galvanostatic mode was used in all electrochemical cycling.  
46  
47 The voltage window was between 0.01-1.2 V. The particle with a limited discharge capacity was also  
48  
49 tested to study the microstructure change along with cycles of the materials.  
50  
51  
52  
53  
54  
55  
56  
57  
58  
59  
60

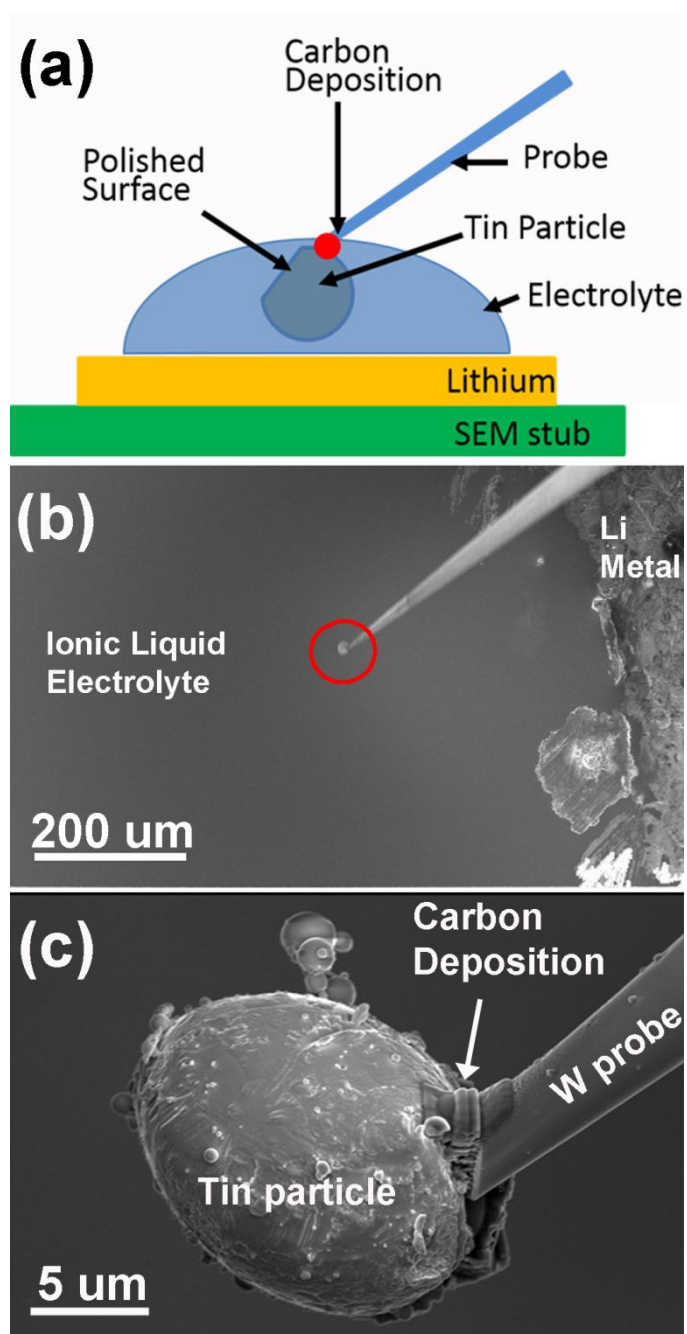


Figure 1. a) Schematic of a single Sn particle battery. b) SEM image of a single Sn particle battery showing the ILE and both Li and Sn electrodes. c) SEM image of a Sn particle attached to a tungsten probe.

As shown in Figure 2, a spherical Sn particle with 10  $\mu\text{m}$  diameter was selected for the experiment. The discharging and charging current was set at 0.3 nA (about C/15 rate). The voltage profile of the

1  
2 first cycle and the estimated relative volume at different states of charge are shown in Figure 2a.  
3  
4  
5 Figures 2b-k are SEM micrographs corresponding to the time points b-k in Figure 2a respectively. At  
6  
7  
8 these points, the galvanostatic discharging or charging was stopped, the particle was lifted out of ILE  
9  
10 and polished by FIB, and then SEM images were taken on the polished surface. The voltage profile  
11  
12 shows that the FIB polishing had a small impact on the cycling performance. After each polishing,  
13  
14 the voltage curve was disturbed a little but quickly returned to the normal level. The voltage profile  
15  
16 does not show the typical three plateaus as reported in the literatures, instead it shows a long plateau  
17  
18 at 0.4 V. In order to understand this phenomenon, we have to eliminate the possible impact of FIB  
19  
20 polishing and imaging on the voltage profile. A Sn particle was cycled at 0.15 nA without FIB  
21  
22 polishing and imaging and the voltage profile also shows a long plateau in the lithiation process  
23  
24 (Figure S1a). This long plateau in the first lithiation process has been observed in Sn film electrodes  
25  
26 <sup>21-23</sup> and it was considered as the result of disorder in the initially formed material. <sup>21</sup> However, the  
27  
28 voltage profile of Sn electrode made of the same Sn particles shows three plateaus in the first lithiation  
29  
30 process (Figure S1b). It means that the long plateau in the first lithiation is not due to the disorder in  
31  
32 the initially formed material. We believe that this phenomenon could be due to the large difference  
33  
34 in Li diffusivity between Li-poor phases and Li-rich phases. As shown in Ref<sup>24</sup>, the diffusivity of Li  
35  
36 in Li-poor phases (before LiSn) is about one order lower than that in Li-rich phases. Due to the high  
37  
38 diffusivity in Li-rich phases and low diffusivity in Li-poor phases (the first and the second plateaus),  
39  
40 it is favorable to form Li-rich phases (the third plateau). As shown in Ref<sup>25-26</sup>, when the size of Sn  
41  
42 particles is larger and the current density is higher, the single plateau appears in the first lithiation.  
43  
44 They have attributed this phenomenon to the slow diffusion rates of Li in Li-poor phases. As shown  
45  
46 in Ref<sup>21-23</sup>, the plateaus appear in the second lithiation. We believe it is due to two reasons. The first  
47  
48 reason is the significant surface area increase due to the pulverization, which results in low current  
49  
50  
51  
52  
53  
54  
55  
56  
57  
58  
59  
60

density on the Sn surface. The second reason is the inhomogeneity of the pulverized Sn material.

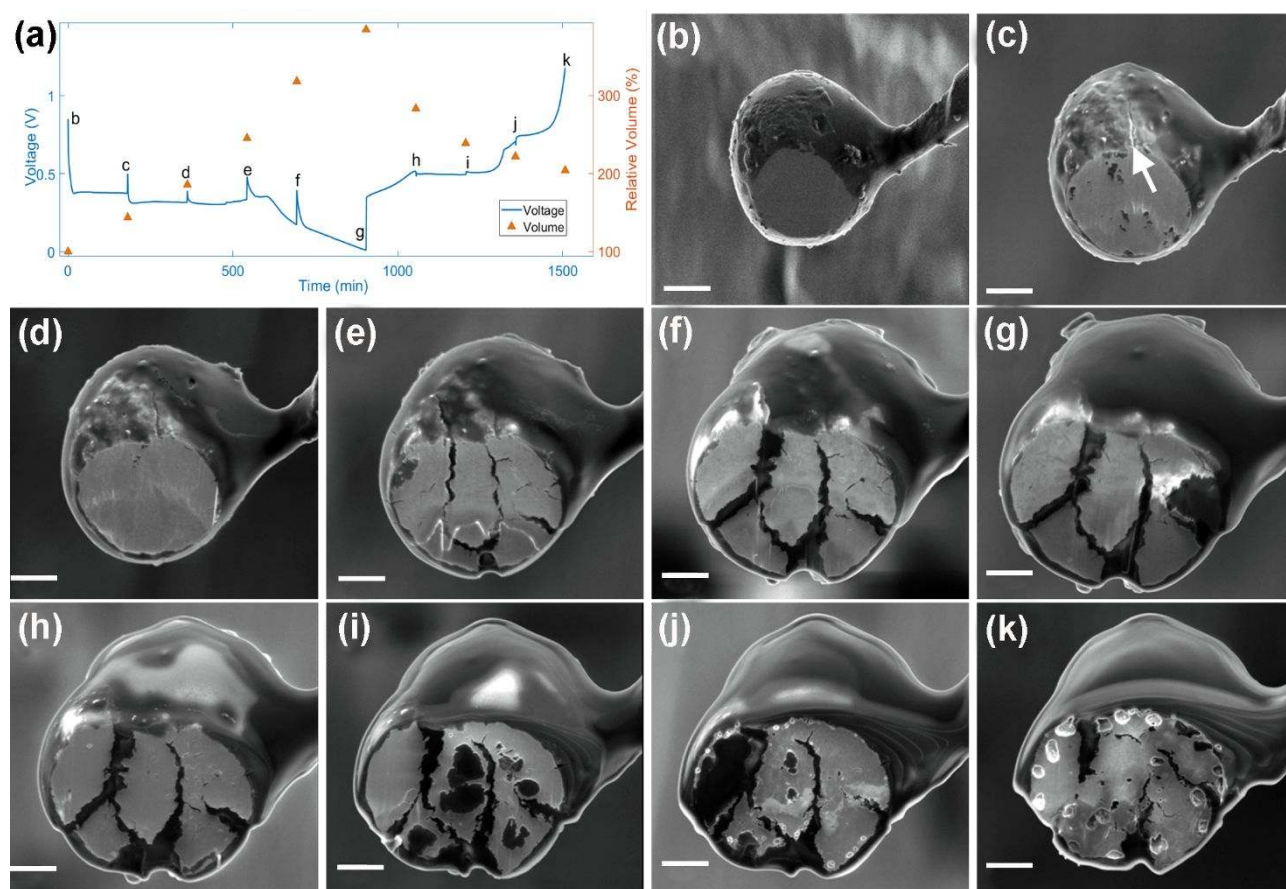


Figure 2. A Sn particle fully discharged/charged at 0.3 nA. a) Voltage profile and relative volume of the first cycle. b) SEM image of as-prepared Tin particle. c-g) SEM images of the same particle at 20%, 40%, 60%, 77% and 100% of discharge states respectively. h-k) SEM images at 25%, 50%, 75% and 100% of charge states respectively. Scale bar is 3  $\mu\text{m}$ .

The relative volume in Figure 2a is estimated by images taken in FIB mode shown in Figure S2.

Figure 2b shows the SEM image of particle before cycling. Figures 2c – g show the SEM images at 20%, 40%, 60%, 77% and 100% of lithiation process and the relative volumes are 144%, 186%, 246%, 318%, and 384%, respectively. These images show an increased degree of cracking of the

1  
2  
3 particle. In Figure 2c, the volume of the particle increased to 144% and a small crack appeared above  
4  
5 the polished surface as indicated by the arrow. On the polished surface, a few concave areas appeared.  
6  
7 In Figure 2d, these concave areas are removed during polishing, which means they are not deep cracks.  
8  
9 In the same image, we can see that small cracks start to appear on the surface. In Figures 2e-g, the  
10  
11 cracks keep growing and propagate into the particle. In Figure 2g, a dark area appears on the right  
12  
13 side of the particle. We believe that it is not a big crack and it is a big concave area due to the  
14  
15 expansion of the material. The volume expansion of particle is almost homogeneous in the first 60%  
16  
17 of lithiation (Figures 2c, d and e). When the cracks become larger (Figures 2f and g), the expansion  
18  
19 is not uniform due to the loss of continuity. At fully lithiated state (figure 2g), the estimated relative  
20  
21 volume is 384%, close to the theoretical value 358%.<sup>27</sup> The delithiation process takes about 10 hours.  
22  
23 SEM images were taken at the beginning and the end of the first plateau, at the end of the second  
24  
25 plateau, and at the end of delithiation process, which are shown in Figures 2h – k. From points h to  
26  
27 k, the relative volumes are 283%, 239%, 222% and 204%. At the beginning of the first plateau (point  
28  
29 h), the relative volume has a large decrease from 384% to 283%. As the delithiation process is close  
30  
31 to the end of the first plateau (point i), some concave areas appeared due to the large contraction of  
32  
33 the material. At the end of the second plateau (point j), it is observed that some nanometer-sized pores  
34  
35 start to appear mainly on the edge of the pulverized particle pieces. At the end of the delithiation  
36  
37 process, the nanopores became larger, but the majority of the pores are on the edge of the pulverized  
38  
39 particle pieces. As discussed in Ref<sup>5, 13</sup>, the formation of pores is due to vacancy-mediated diffusion  
40  
41 during the delithiation process. Our results show that the pores do not appear in the first plateau  
42  
43 (transition from  $\text{Li}_{22}\text{Sn}_5$  to  $\text{LiSn}$ ). They start to form in the second plateau (transition from  $\text{LiSn}$  to  
44  
45  $\text{Li}_2\text{Sn}_5$ ). The pores become larger in the third plateau probably due to the merging of pores, which is  
46  
47 the transition from  $\text{Li}_2\text{Sn}_5$  to  $\text{Sn}$ . It could be due to the large difference of Li diffusivity in Li-rich and  
48  
49  
50  
51  
52  
53  
54  
55  
56  
57  
58  
59  
60



1  
2  
3 Li-poor phases. From points i to k, the relative volume has relatively small change from 239% to  
4  
5 204%. We believe that it is mainly due to the formation of pores. To verify that the formation of pores  
6  
7 are not affected by the FIB polishing process, after the first cycle, we polished the particle from the  
8  
9 other side. The morphology of the polished surface is shown in Figure S3. The FIB-SEM tomography  
10  
11 was employed to reveal the porous structure in 3D as shown in Figure S4. The 3D image shows pores  
12  
13 distributed across the particle. The larger pores are still mainly in the areas close to the edge of the  
14  
15 pulverized particle pieces.  
16  
17  
18  
19  
20  
21  
22  
23  
24

25 The same particle was transferred to a TEM grid after the above steps and a TEM specimen was  
26  
27 prepared (Figure 3a). A JEOL JEM2100F TEM was employed for the microstructure analysis. Figure  
28  
29 3b is a low magnification micrograph of the area around a crack and a pore. Figures 3c and d are  
30  
31 distribution of Sn and Li by energy-filtered TEM (EFTEM). The brighter means there is relatively  
32  
33 more element. The result shows that Sn is uniformly distributed in the whole area. But Li is mainly  
34  
35 distributed at the edge of the crack and the pore. Figure 3e is a high resolution TEM (HREM) image  
36  
37 near the crack. There is a clear boundary between the crystal Sn and the amorphous  $\text{Li}_x\text{Sn}$ . Figure 3f  
38  
39 is the electron diffraction pattern of Sn which indicates the tin's crystal structure recovered after the  
40  
41 delithiation process.  
42  
43  
44  
45  
46  
47  
48  
49  
50  
51  
52  
53  
54  
55  
56  
57  
58  
59  
60

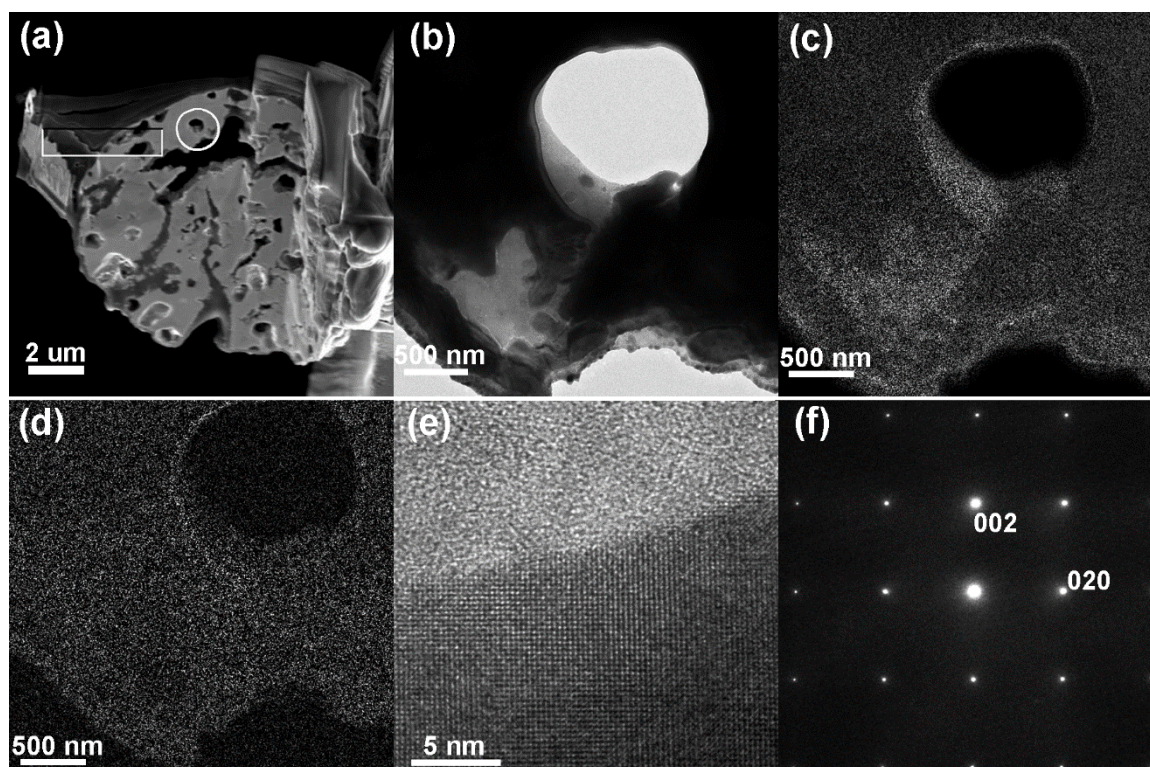


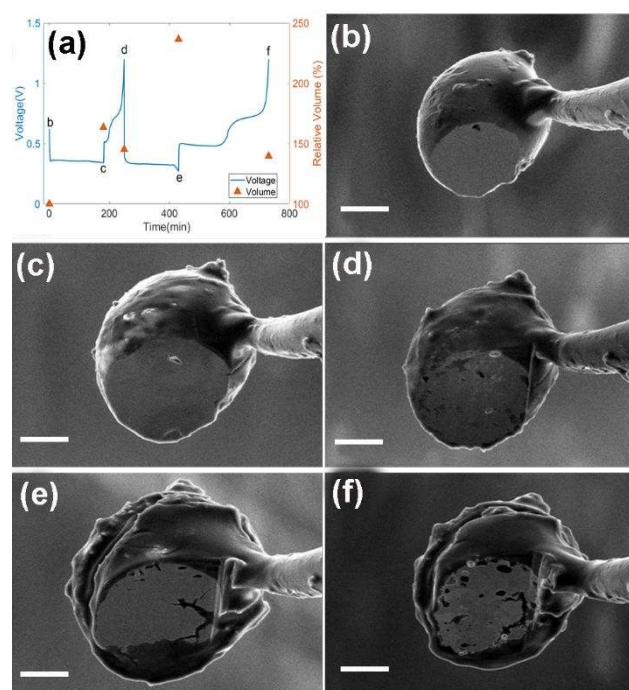
Figure 3. (a) SEM image of TEM sample after the final thin milling. (b) TEM image of the circled area in (a). (c) EFTEM mapping of Li. (d) EFTEM mapping of Sn. (e) HREM image near the crack. (f) Electron diffraction pattern of Sn.

In order to investigate the microstructural evolution under cycling and the potential capacity fading mechanisms, the same particle used to obtain the voltage profile shown in Figure S1a was cycled at 0.75 nA after the first cycle at 0.15 nA. As shown in Figure S5a, the capacity did not degrade after five cycles. It even increased a little in five cycles. It could be due to more complete lithiation of the Sn particle at high current when the surface area was increased during pulverization. However, Figures S5b and c show that the morphology of the particle is changed from a spherical shape with a smooth surface to an irregular shape with a rough surface. Figure S5d shows that the internal microstructure has become a completely porous structure. We can expect that the particle will pulverize completely and start to lose capacity when the cycling continues.

1  
2  
3  
4  
5  
6 We also tested a Sn particle at higher current of 1.5 nA (about 3/5 C rate). The voltage profile,  
7  
8 relative volume and SEM images at different states of charge are shown in Figure S6. The evolution  
9  
10 of microstructure is similar to the particle tested at 0.3 nA. Cracks appear and increase during the  
11  
12 lithiation process, porous structures are formed during the delithiation process. Due to the high current,  
13  
14 the particle didn't reach its full discharge capacity. The relative volume is 255% at the end of lithiation  
15  
16 process. We also can see that the third plateau in the delithiation process is very short. It means that  
17  
18 the transition from  $\text{Li}_2\text{Sn}_5$  to Sn is very short and most of the materials remain as  $\text{Li}_2\text{Sn}_5$  or LiSn  
19  
20 phases. As shown in Figure S6f, at the end of delithiation, the pores are not as large as the pores  
21  
22 shown in Figures S3. It confirms that the merging of nanopores happens in the third plateau during  
23  
24 the transition from  $\text{Li}_2\text{Sn}_5$  to Sn.  
25  
26  
27  
28  
29  
30  
31  
32  
33  
34  
35

36 It has been proposed that limiting the degree of Li uptake to the stoichiometry of LiSn relieves  
37  
38 the pulverization problem to some extent. As shown in Figure 4, a Sn particle was tested with a limited  
39  
40 discharge capacity of 0.9 nAh at 0.3 nA current. The particle was tested for two cycles. Figure 4a  
41  
42 shows the voltage profile and relative volume. Figure 4b shows the particle in as-prepared condition.  
43  
44 Figures 4c – f represent the same particle after the first discharging, the first charging, the second  
45  
46 discharging and the second charging. Scanning ion beam images (Figures S7b-f) taken during cycling  
47  
48 and SEM images (Figures S7g-h) taken from another angle after cycling illustrate the microstructural  
49  
50 evolution. After the first discharging process, small cracks occur on the particle, but the polished  
51  
52 surface is still intact. After the first charging, concave areas and pores start to appear on the polished  
53  
54 surface. However, as shown in Figure 4a, only 38% of Li was removed from the particle and the  
55  
56  
57  
58  
59  
60

1  
2  
3 relative volume is decreased from 163% to 145%. It is probably due to the low Li diffusivity of Li-  
4  
5 poor phases, which are the majority of Li-Sn alloy in this case. After the second discharging, the small  
6  
7 cracks, which appeared during the first discharging propagate into the particle and more cracks are  
8  
9 formed on the polished surface. After the second charging, porous structures are clearly shown on the  
10  
11 particle. After the second cycle, the Li left in the particle in the first cycle is almost completely  
12  
13 removed. We believe that it is due to the pulverization of the particle, which increases the active  
14  
15 surface area and the inhomogeneity.  
16  
17  
18  
19  
20



21  
22  
23  
24  
25  
26  
27  
28  
29  
30  
31  
32  
33  
34  
35  
36  
37  
38  
39  
40  
41  
42  
43  
44  
45  
46  
47  
48  
49  
50  
51  
52  
53  
54  
55  
56  
57  
58  
59  
60

Figure 4. A Sn particle cycled with 0.9 nAh discharge limit and 0.3 nA current. a) Voltage profile and relative volume of the first two cycles. b-f) SEM images of the particle at the as-prepared, the first discharged, the first charged, the second discharged and the second charged states, respectively. Scale bar is 3  $\mu\text{m}$ .

In summary, a single Sn particle battery cell has been built in the chamber of a FIB-SEM with vacuum environment by using ionic liquid electrolyte. This in situ cell provides a direct way to

1  
2  
3 measure and correlate the electrochemical performance and microstructural evolution of single Sn  
4  
5 particle during cycling. Our results show the formation and evolution of cracks and porous structures  
6  
7 at different states of charge during lithiation/delithiation processes. The electrochemical  
8  
9 characteristics of the Sn particle are clearly affected by the microstructural evolution. This method is  
10  
11 promising in the study of batteries to understand electrochemical reactions and mechanical  
12  
13 degradation of high capacity battery materials.  
14  
15  
16  
17  
18  
19  
20  
21

## 22 **Acknowledgements**

23  
24  
25 This work was supported by the US National Science Foundation under Grant No. 1603847. This  
26  
27 work was performed, in part, at the Center for Nanoscale Materials, an Office of Science user facility,  
28  
29 was supported by the U.S. Department of Energy, Office of Science, Office of Basic Energy Sciences,  
30  
31 under Contract No. DE-AC02-06CH11357.  
32  
33  
34  
35  
36  
37  
38

## 39 **ASSOCIATED CONTENT**

40  
41 Supporting Information available: [Comparison of the voltage profiles between a coin cell with Sn  
42  
43 electrode and a single Sn particle cell, FIB images of a Sn particle fully discharged/charged at 0.3  
44  
45 nA, SEM image of the other side of a Sn particle fully discharged/charged at 0.3 nA, 3D reconstructed  
46  
47 microstructure of the Sn particle shown in Figure 2, SEM images of a Sn particle after 6 cycles, SEM  
48  
49 images of a Sn particle cycled at 1.5 nA, and FIB images of a Sn particle with limited discharge  
50  
51 capacity.]  
52  
53  
54  
55  
56  
57  
58  
59  
60

## References

1. Kamali, A.; Fray, D. J., *Tin-based materials as advanced anode materials for lithium ion batteries: A review*. 2011; Vol. 27.
2. Beaulieu, L.; Eberman, K.; Turner, R.; Krause, L.; Dahn, J., Colossal reversible volume changes in lithium alloys. *Electrochem. Solid-State Lett.* **2001**, *4* (9), A137-A140.
3. Zhang, M.; Wang, T.; Cao, G., Promises and challenges of tin-based compounds as anode materials for lithium-ion batteries. *Int. Mater. Rev.* **2015**, *60* (6), 330-352.
4. Dang, H. X.; Klavetter, K. C.; Meyerson, M. L.; Heller, A.; Mullins, C. B., Tin microparticles for a lithium ion battery anode with enhanced cycling stability and efficiency derived from Se-doping. *J. Mater. Chem. A* **2015**, *3* (25), 13500-13506.
5. Chao, S.-C.; Song, Y.-F.; Wang, C.-C.; Sheu, H.-S.; Wu, H.-C.; Wu, N.-L., Study on Microstructural Deformation of Working Sn and SnSb Anode Particles for Li-Ion Batteries by in Situ Transmission X-ray Microscopy. *The Journal of Physical Chemistry C* **2011**, *115* (44), 22040-22047.
6. Li, T.; Kang, H.; Zhou, X.; Lim, C.; Yan, B.; De Andrade, V.; De Carlo, F.; Zhu, L., Three-Dimensional Reconstruction and Analysis of All-Solid Li-Ion Battery Electrode Using Synchrotron Transmission X-ray Microscopy Tomography. *ACS Applied Materials & Interfaces* **2018**, *10* (20), 16927-16931.
7. Sun, F.; Markötter, H.; Zhou, D.; Alrwashdeh Saad Sabe, S.; Hilger, A.; Kardjilov, N.; Manke, I.; Banhart, J., In Situ Radiographic Investigation of (De)Lithiation Mechanisms in a Tin-Electrode Lithium-Ion Battery. *ChemSusChem* **2016**, *9* (9), 946-950.
8. Wang, J.; Chen-Wiegart Yu-chen, K.; Wang, J., In Situ Three-Dimensional Synchrotron X-Ray Nanotomography of the (De)lithiation Processes in Tin Anodes. *Angewandte Chemie International Edition* **2014**, *53* (17), 4460-4464.
9. Weker, J. N.; Liu, N.; Misra, S.; Andrews, J. C.; Cui, Y.; Toney, M. F., In situ nanotomography and operando transmission X-ray microscopy of micron-sized Ge particles. *Energy & Environmental Science* **2014**, *7* (8), 2771-2777.
10. Hua, L. X.; Yang, L.; Akihiro, K.; Sulin, Z.; Ting, Z.; Ju, L.; Yu, H. J., In Situ TEM Experiments of Electrochemical Lithiation and Delithiation of Individual Nanostructures. *Advanced Energy Materials* **2012**, *2* (7), 722-741.
11. Li, Q.; Wang, P.; Feng, Q.; Mao, M.; Liu, J.; Mao, S. X.; Wang, H., In Situ TEM on the Reversibility of Nanosized Sn Anodes during the Electrochemical Reaction. *Chemistry of Materials* **2014**, *26* (14), 4102-4108.
12. Liu, X. H.; Huang, J. Y., In situ TEM electrochemistry of anode materials in lithium ion batteries. *Energy & Environmental Science* **2011**, *4* (10), 3844-3860.
13. Wang, J.; Fan, F.; Liu, Y.; Jungjohann, K. L.; Lee, S. W.; Mao, S. X.; Liu, X.; Zhu, T., Structural Evolution and Pulverization of Tin Nanoparticles during Lithiation-Delithiation Cycling. *Journal of The Electrochemical Society* **2014**, *161* (11), F3019-F3024.
14. Cook, J. B.; Lin, T. C.; Detsi, E.; Weker, J. N.; Tolbert, S. H., Using X-ray Microscopy To Understand How Nanoporous Materials Can Be Used To Reduce the Large Volume Change in Alloy Anodes. *Nano Letters* **2017**, *17* (2), 870-877.
15. Huang, J. Y.; Zhong, L.; Wang, C. M.; Sullivan, J. P.; Xu, W.; Zhang, L. Q.; Mao, S. X.; Hudak, N. S.; Liu, X. H.; Subramanian, A.; Fan, H.; Qi, L.; Kushima, A.; Li, J., In Situ Observation of the Electrochemical Lithiation of a Single SnO<sub>2</sub> Nanowire Electrode. *Science* **2010**, *330* (6010), 1515.
16. Chen, C.-Y.; Sano, T.; Tsuda, T.; Ui, K.; Oshima, Y.; Yamagata, M.; Ishikawa, M.; Haruta, M.; Doi, T.; Inaba, M.; Kuwabata, S., In situ Scanning Electron Microscopy of Silicon Anode Reactions

- 1  
2 in Lithium-Ion Batteries during Charge/Discharge Processes. *Scientific Reports* **2016**, *6*, 36153.
- 3 17. Marceau, H.; Kim, C.-S.; Paoletta, A.; Ladouceur, S.; Lagacé, M.; Chaker, M.; Vijn, A.; Guerfi,  
4 A.; Julien, C. M.; Mauger, A.; Armand, M.; Hovington, P.; Zaghbi, K., In operando scanning electron  
5 microscopy and ultraviolet–visible spectroscopy studies of lithium/sulfur cells using all solid-state  
6 polymer electrolyte. *Journal of Power Sources* **2016**, *319*, 247-254.
- 7 18. Miller, D. J.; Proff, C.; Wen, J. G.; Abraham, D. P.; Bareño, J., Observation of Microstructural  
8 Evolution in Li Battery Cathode Oxide Particles by In Situ Electron Microscopy. *Advanced Energy*  
9 *Materials* **2013**, *3* (8), 1098-1103.
- 10 19. Galiński, M.; Lewandowski, A.; Stępnik, I., Ionic liquids as electrolytes. *Electrochimica Acta*  
11 **2006**, *51* (26), 5567-5580.
- 12 20. Lewandowski, A.; Świdarska-Mocek, A., Ionic liquids as electrolytes for Li-ion batteries—An  
13 overview of electrochemical studies. *Journal of Power Sources* **2009**, *194* (2), 601-609.
- 14 21. Yang, S.; Zavalij, P. Y.; Whittingham, M. S., Anodes for lithium batteries: tin revisited.  
15 *Electrochem. Commun.* **2003**, *5* (7), 587-590.
- 16 22. Cui, Y.; Li, T.; Zhou, X.; Mosey, A.; Guo, W.; Cheng, R.; Fu, Y.; Zhu, L., Electrochemical  
17 behavior of tin foil anode in half cell and full cell with sulfur cathode. *Electrochimica Acta* **2019**,  
18 *294*, 60-67.
- 19 23. Tamura, N.; Ohshita, R.; Fujimoto, M.; Fujitani, S.; Kamino, M.; Yonezu, I., Study on the anode  
20 behavior of Sn and Sn–Cu alloy thin-film electrodes. *J. Power Sources* **2002**, *107* (1), 48-55.
- 21 24. Winter, M.; Besenhard, J. O., Electrochemical lithiation of tin and tin-based intermetallics and  
22 composites. *Electrochim. Acta* **1999**, *45* (1-2), 31-50.
- 23 25. Wachtler, M.; Winter, M.; Besenhard, J. O., Anodic materials for rechargeable Li-batteries.  
24 *Journal of Power Sources* **2002**, *105* (2), 151-160.
- 25 26. Yang, J.; Takeda, Y.; Imanishi, N.; Yamamoto, O., Ultrafine Sn and SnSb<sub>0.14</sub> Powders for  
26 Lithium Storage Matrices in Lithium-Ion Batteries. *Journal of The Electrochemical Society* **1999**,  
27 *146* (11), 4009-4013.
- 28 27. Ichitsubo, T.; Yukitani, S.; Hirai, K.; Yagi, S.; Uda, T.; Matsubara, E., Mechanical-energy  
29 influences to electrochemical phenomena in lithium-ion batteries. *Journal of Materials Chemistry*  
30 **2011**, *21* (8), 2701-2708.
- 31  
32  
33  
34  
35  
36  
37  
38  
39  
40  
41  
42  
43  
44  
45  
46  
47  
48  
49  
50  
51  
52  
53  
54  
55  
56  
57  
58  
59  
60

## Table of Contents graphic

